

CHARACTERIZATION OF SPIN-COATED TiO₂ BUFFER LAYERS FOR DYE-SENSITIZED SOLAR CELLS

J. LUNGU^a, N. ȘTEFAN^b, G. PRODAN^a, A. GEORGESCU^a, A. MANDEȘ^a,
V. CIUPINĂ^{a,c}, I. N. MIHĂILESCU^{b,c}, M. A. GÎRȚU^{a*}

^a*Department of Physics, Ovidius University of Constanța, Constanța 900527, Romania*

^b*National Institute for Lasers, Plasma and Radiation Physics, (Lasers Department), Atomiștilor 409, P.O. Box MG-36, RO-077125 Bucharest-Măgurele, Romania*

^c*Faculty of Physics, University of Bucharest, Atomiștilor 405, P. O. Box MG-11, 077125, Bucharest-Măgurele, Romania*

We report results on the fabrication and testing of dye-sensitized solar cells (DSSC) with spin coated TiO₂ thin films used as intermediate buffer layer between the conductive glass substrate and the nanocrystalline TiO₂ mesoporous layer. Our goal is to improve the DSSC characteristic parameters, such as the short circuit current density and the overall photovoltaic conversion efficiency. The oxide was prepared as thin transparent film from sol-gel Ti(i-OPr)₄ ethanolic solution, which was spin coated at 7000 rpm on top of the fluorine doped SnO₂ (FTO) glass. The basic properties of the films were characterized by complementary techniques. The structure and crystallinity of the TiO₂ intermediate layer were investigated by transmission electron microscopy (TEM) associated with selected area electron diffraction (SAED) and high resolution transmission electron microscopy (HRTEM). We found experimentally that the TiO₂ buffer layer can lead to an increase by a factor of more than 2.5 for the short circuit current density. Moreover, the photovoltaic conversion efficiency, measured under standard AM 1.5G conditions, was overall increased twofold.

(Received June 29, 2015; Accepted August 17, 2015)

Keywords: TiO₂ thin film, buffer layer, Spin coating, Dye-sensitized solar cells, Photovoltaic conversion efficiency

1. Introduction

The spin-coating technique is one of the most popular methods for applying thin uniform films onto flat surfaces. It is used frequently in photovoltaic research, due to its ease of use and relatively low cost, although it is not suitable for large-scale film processing [1]. In brief, an excess amount of a solution is placed on the substrate, which is then rotated at high speed in order to spread the fluid by centrifugal force. This method of spin coating was first described by Emslie et al. [2] and Meyerhofer et al. [3] using several simplifications. There are several steps in the spinning process, including deposition of the coating fluid onto the wafer or a flat substrate, accelerating the substrate up to its final, desired, rotational speed, spinning of the substrate in order for the fluid viscous forces to dominate the fluid thinning behavior, and evaporation of the solvent. The spin coating process generates a solid film. In order to get homogeneous films, several different factors are important and have to be considered: evaporation rate of the solvent,

*Corresponding author: mihai.girtu@univ-ovidius.ro

viscosity of the fluid, concentration of the solution, angular velocity (rotating speed) and spinning time.

Regarding the evaporation rate of the solvent, it is necessary to have a solvent that evaporates fast at room temperature. The evaporation process influences the flow of the solution. Thus, a volatile solvent leads to a viscous solution and a thick film.

Another factor influencing the spin coating process is the interactions between substrate and solution layer, even stronger than the interactions between solution surface layer and air.

The film thickness is dependent on the viscosity and concentration of the liquid. The more concentrated the solution is, the thicker the film. The film thickness also depends on the angular velocity. The same dependency is obtained for the spinning time. The longer the spinning time is, the smaller the film thickness, for constant spinning speed [4,5].

In this work, we spin-coat a TiO_2 compact film at the interface between the $\text{SnO}_2\text{:F}$ (FTO) conducting glass and the TiO_2 mesoporous layer in dye-sensitized solar cells (DSSC), to enhance the cell performance [6-11]. The TiO_2 buffer layer is obtained by spin coating a sol-gel titanium (IV) isopropoxide-based solution diluted with ethanol on the FTO glass. The buffer layer is expected [8] to reduce the recombination of electrons at the electrode/electrolyte interface, to protect the electrodes against the action of the dye solution, and to ensure a better contact between the TiO_2 layer and FTO substrate. Here, we study the influence of the buffer layer on the short circuit current density and on the photovoltaic conversion efficiency of the DSSCs.

2. Experimental

The conductive glass substrates consisting of soda lime glass sheet of 2.2 mm thickness, covered with a conductive layer of fluorine-doped tin oxide ($\text{SnO}_2\text{:F}$) (FTO) with a 7 ohm/square resistivity (Solaronix) were ultrasonically cleaned 15 minutes each in acetone, ethanol and de-ionized water, to remove any traces of impurities, and then air dried. This procedure was followed by spin-coating an intermediate thin film, as buffer layer, prior to the deposition of the active layer of mesoporous TiO_2 . The intermediate layer was prepared as thin transparent film from sol-gel titanium (IV) isopropoxide ($\text{Ti}[\text{OCH}(\text{CH}_3)_2]_4$, Aldrich) ethanolic solution.

Using a magnetic stirrer we mixed 2.5 ml $\text{Ti}[\text{OCH}(\text{CH}_3)_2]_4$ with 1.75 ml acetylacetone (Fluka). Due to the highly exothermic reaction, acetylacetone was added dropwise with constant stirring, to the titanium isopropoxide solution to avoid drastic temperature increase. Over the obtained solution we added 12.75 ml EtOH and the color of the solution became orange-yellow [12,13].

The spin-coating of the TiO_2 sol-gel ethanolic solution was carried out in air with a spinning speed of 7000 rpm for 3 s. The precursor film formed following the deposition process was dried at 240°C for 1 min on a hot plate. Heat treatment at 240°C is recommended because the boiling point of acetyl acetone is 136-138°C and that of $\text{Ti}[\text{OCH}(\text{CH}_3)_2]_4$ is 232°C [14], which leads to the complete evaporation of the organic compounds, and to initiate the formation and crystallization of TiO_2 blocking layer. The spinning – drying cycle was repeated two, four, six, eight and ten times in order to get films of different thickness [15]. The films with 2, 4, 6, 8, and 10 spin-coated layers were denoted T2X, T4X, T6X, T8X and T10X, respectively. After the deposition of last coating layer, the resulting film was annealed in air at 450°C for 1 h and the thin TiO_2 surface was transparent and had a light-blue color.

The films thicknesses were analyzed in the thickness range 15 nm - 70 μm and the wavelength range 380-1050 nm, using a Spectral Reflectance (SR) instrument, Filmatrix F20 thin-film analyzer. The optical properties were analyzed in the range 300–1200 nm, using an UV-Vis-NIR spectro-photometer, model *Cintra 10e*. The morphology and the structural properties of the deposited films were investigated by transmission electron microscopy (TEM) associated with selected area electron diffraction (SAED) and high transmission electron microscopy (HRTEM),

using an electron microscope *TEM Philips CM 120 ST* operating at 120 kV and having a point-to-point resolution of 0.24 nm.

DSSCs were fabricated using the photoelectrodes with different numbers of buffer layers. The TiO_2 paste was obtained by applying the Pechini type sol-gel method starting from a polyester-based titanium sol consisting in a mixture of precursor with molar ratio of 1:4:16 {[$\text{Ti}[\text{OCH}(\text{CH}_3)_2]_4$: citric acid: ethylene glycol}]. The paste has been prepared by grinding the nanocrystalline anatase TiO_2 powder (P25, Sigma-Aldrich) and the sol-gel solution with 7:1 molar ratio between TiO_2 and [$\text{Ti}[\text{OCH}(\text{CH}_3)_2]_4$] [16,17] in a mortar. The coating was carried out on the TiO_2 blocking layer by doctor blade technique, followed by sintering at 450°C for 1h in air and left to cool down to room temperature [11].

The final step in obtaining the photoelectrodes consisted in sensitization of nanostructured TiO_2 with the N719 (Ruthenium 535-bisTBA) pigment, cis-diisothiocyanato-bis(2,20-bipyridyl-4,40-carboxylato ruthenium(II) bis(tetrabutylammonium) [18] (Solaronix) 0.2mM in absolute ethanol, by soaking at 80°C for 2 h. The plate was rinsed with absolute ethanol to remove the excess dye and dried for 10 min at 80°C.

Platinum counter electrodes were prepared by spreading a few droplets of Platisol T (Solaronix) onto the conductive glass, followed by heating at 450°C for 10 minutes. All photoelectrode and counterelectrode plates were stored in desiccators before use. To assemble the DSSCs, the plates were secured together with small bulldog clips [19,20]. The liquid electrolyte (Iodolyte Z-50, Solaronix) is drawn into the space between the electrodes by capillary action.

The electro-optical parameters of the DSSCs, mainly the fill factor, FF , the photovoltaic conversion efficiency, η , the short circuit current, I_{SC} , and the open circuit voltage, V_{OC} , of the photovoltaic cells were measured under AM 1.5G standard sun conditions (1000W/m²) at 25°C, using a class A small area solar simulator [21]. The cell surface was exposed to light through a circular slit of 10 mm diameter, resulting in a useful area of about 0.785 cm². The current and voltage values were measured using two digital bench multimeters (*Mastech MS8050*) and a decadic precision resistance box. All measurements were made at about 45 s intervals, allowing time for each reading to stabilize.

3. Results and discussion

3.1. Characterization of the TiO_2 thin film

The thicknesses of the spin-coated TiO_2 films are reported as a function of the number of layers (see Fig. 1).

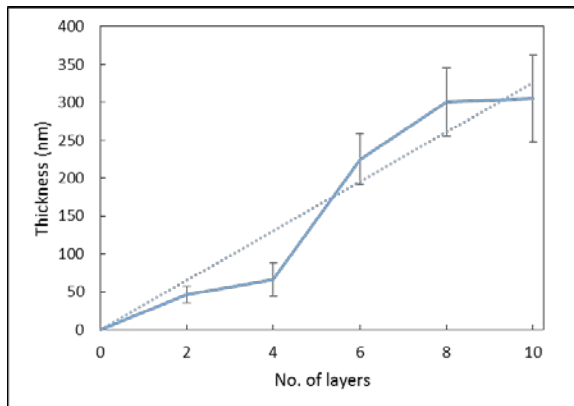


Fig. 1. The thickness of the TiO_2 buffer films as a function of the number of spin-coated layers. The dotted line is a linear fit.

As expected, the film thickness after thermal treatment increases with the number of spin-coated layers, from about 47 nm for T2X to around 305 nm for T10X. Although the error of the thickness measurement is less than 2%, the large error bars displayed in Fig. 1 are due to the nonuniformity of the films, possible adherence problems, uneven solvent evaporation during the heating cycle (observed for such ZnO layers [22]), etc. In any case, a correlation between the number of layers and the film thickness is obvious, the fit to a straight line leading to a slope of about 33 nm per layer.

Next, we studied the optical transmittance (Fig. 2) and absorbance spectra (Fig. 3) for the TiO₂ buffer layers. The lowest absorption throughout the visible range is recorded for T2X, whereas all other plates absorb starting from 350 nm (but T2X from Fig. 3 also seems to absorb starting at 350 nm). T10X plate spectrum shape is very similar to that for FTO, the difference in intensity between the two remaining almost constant for all wavelengths. At the UV-Vis limit, the other plates (T4X, T6X and T8X) absorb radiation in about equal measures. T8X plate has the best absorption in the ranges 450-520 nm, 610-690 nm and NIR (850-1200 nm), while for T6X the reverse situation is registered, as it absorbs only slightly better in the range 510-600 nm.

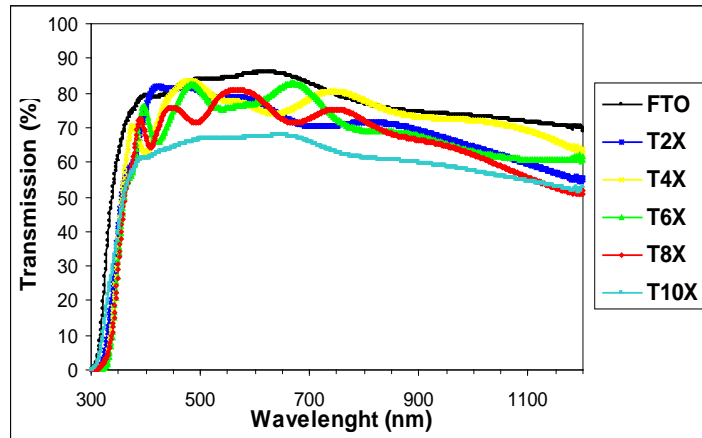


Fig. 2. The transmission spectra of the spin-coated TiO₂ buffer layers of various thicknesses, compared to the bare FTO glass.

The steep decrease of the transparency in the near-UV region is caused by the strong light absorption in TiO₂, which is a wide bandgap semiconductor with the gap opening in the near UV, of about 3.2 eV [23].

The wavelengths where the decrease in transmittance occurs are about 380 nm for all “TX” labeled plates, whereas for the FTO glass the wavelength is ~370 nm. The bandgap energy E_g of about 3.35 eV of the films was obtained by fitting the spectra to the equation of the absorption coefficient α , which is valid in the absence of the scattering effects and for allowed indirect optical transitions [24],

$$\alpha \sim (E - E_g)^2, \quad (4)$$

where E is the photon energy. The slight increase in E_g may be correlated with finite size effects in the nanostructured photoelectrodes.

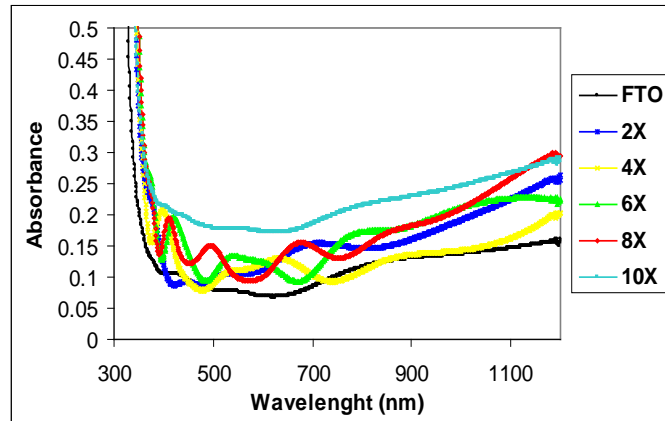


Fig. 3. The absorption spectra of the spin-coated TiO_2 buffer layers of various thicknesses, compared to the bare FTO glass.

Figs. 4-9 show transmission electron microscopy (TEM) images, grain size histograms (lognormal fitted), selected area electron diffraction (SAED) patterns and high transmission electron microscopy (HRTEM) images for the various spin-coated TiO_2 buffer layers. The grain sizes determined from TEM investigations are in the range of 6-30 nm for T6X TiO_2 , with an average size of 13 nm (Fig. 4 inset), for T8X TiO_2 is in the range of 10-30 nm, with an average size of 15 nm (Fig. 6 inset) and of 18-75 nm for T10X TiO_2 , with an average size of 27 nm (Fig. 8 inset). The associated SAED patterns and HRTEM images show the anatase structure of titania nanoparticles.

The SAED patterns for T6X, T8X and T10X films, presented in the insets of Figs. 5, 7 and 9, show a very intense ring corresponding to reflection from (101) planes which indicates the anatase phase of nanocrystallites, but also some low intensity rings corresponding to reflections from other planes. Those images reveal also the values of interplanar distance of 0.355 nm for T6X, 0.351 nm for T8X and 0.348 nm for T10X, which are rather close to the standard anatase (101) plane (0.351690 nm). At a higher magnification, the TEM images of T6X, T8X and T10X samples exhibit both round shaped and elongated or faceted particles, by different sizes (Fig. 5, 7 and 9 respectively). Anatase phase nanocrystallites can be identified also from the 0.35 nm lattice fringes appearing in the same HRTEM images, which is in perfect agreement with SAED results.

Table 1 presents the comparative experimental values obtained for the distances between lattice planes in SAED analyzes, and the reference values for anatase TiO_2 .

Table 2 summarizes the results obtained from TEM investigation. It should be noted that TEM analysis utilized small portion of the sample and may not always give a representative portrayal of the whole sample [25].

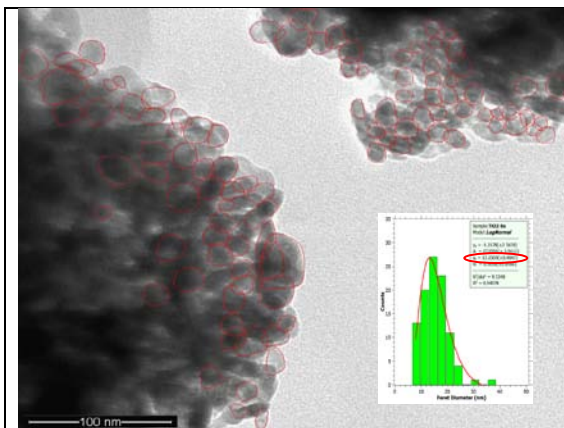


Fig. 4 TEM image with the distribution of grain size corresponding to six layers of TiO_2 (T6X).

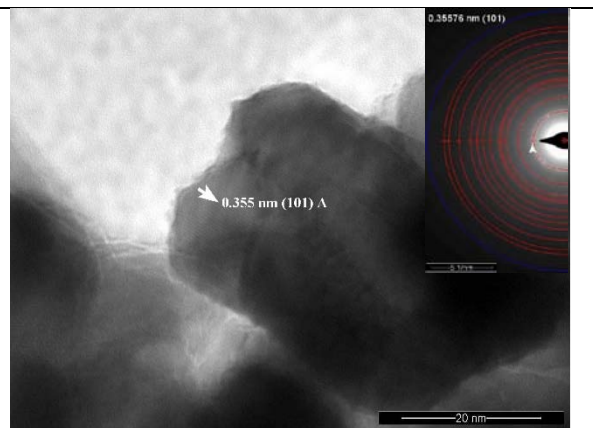


Fig. 5 HRTEM image and ELD patterns for (T6X)

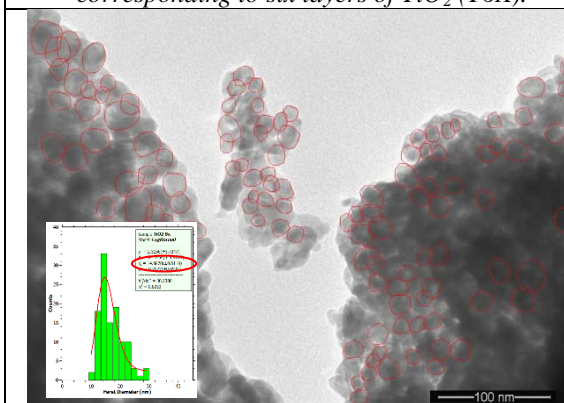


Fig. 6 TEM image with the distribution of grain size corresponding to eight layers of TiO_2 (T8X).

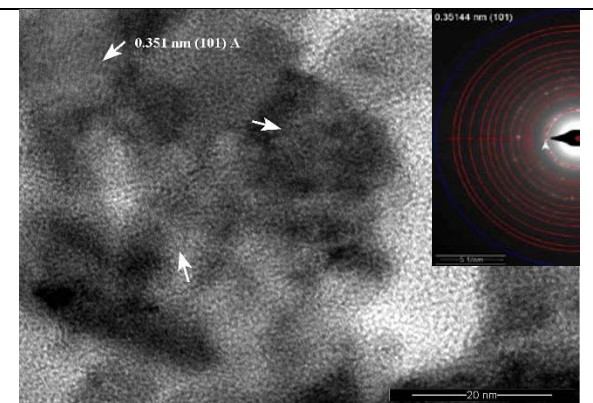


Fig. 7 HRTEM image and ELD patterns for (T8X).

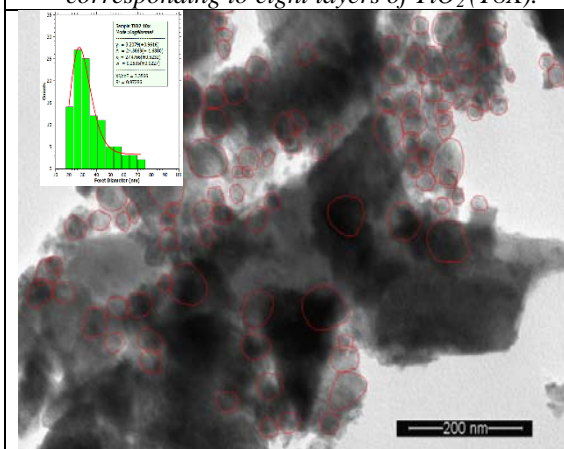


Fig. 8 TEM image with the distribution of grain size corresponding to eight layers of TiO_2 (T10X).

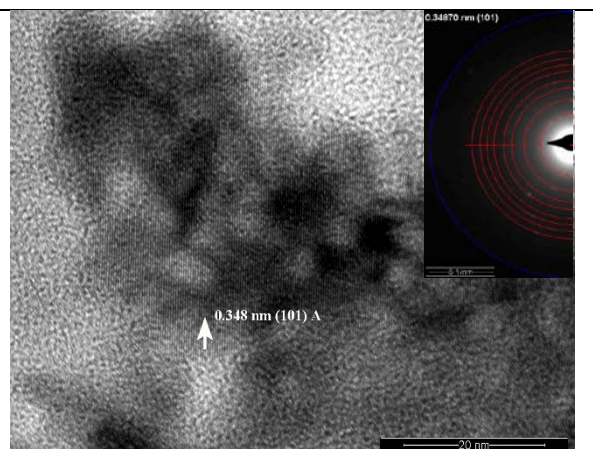


Fig. 9 HRTEM image and ELD patterns for (T10X).

Table 1. Mean crystallite size, in nm, based on TEM investigations for the spin-coated layers.

T6X	13.23 (± 0.48)
T8X	14.68 (± 0.61)
T10X	27.47 (± 0.52)
mesoporous TiO ₂	16.36 (± 0.26)

Table 2. Experimental values for the distances between the lattice planes in SAED analyses, and the reference values for anatase TiO₂.

Peak no.	Present work								Ref.	
	T6X		T8X		T10X		meso. TiO ₂		TiO ₂ anatase	
	d-value (Å)	Scaled intens.	d-value (Å)	Scaled intens.	d-value (Å)	Scaled intens.	d-value (Å)	Scaled intens.	d-value (Å)	Scaled intens.
1*	3.5576	A101	3.5144	A101	3.4870	A101	3.5263	A101	3.5169 0	101
2*	2.4026	A103- A004- A112	2.3646	A103- A004- A112	2.3748	A103- A004- A112	2.3792	A103- A004- A112	2.4308 6 2.3785 0 2.3325 6	103 004 112
3*	1.9106	A200	2.1379	-	1.9098	A200	1.8950	A200	1.8925 0	200
4*	1.7522	A105- A211	1.8948	A200	1.6855	A105- A211	1.7333	A105- A211	1.7000 6 1.6665 3	105 211
5*	1.6958	A105- A211	1.6819	A105- A211	1.4764	A213- A204	1.6775	A105- A211	1.7000 6 1.6665 3	105 211
6*	1.496	A213- A204	1.4790	A213- A204	1.3562	A116- A220	1.4841	A213- A204	1.4933 0 1.4809 2	213 204
7*	1.3625	A116- A220	1.3494	A116- A220	1.2537	A301- A215	1.3503	A116- A220	1.3642 1 1.3382 0	116 220
8*	1.2742	A301- A215	1.2600	A301- A215	1.1588	A224	1.2636	A301- A215	1.2507 2 1.2647 0	301 215
9*	1.1801	A224	1.1659	A224	-	-	1.1689	A224	1.1662 8	224
10*	1.0549	-	1.0434	-	-	-	1.0471	-	-	-
11*	0.963	-	0.9487	-	-	-	1.0196	-	-	-
12*	0.9244	-	0.9038	-	-	-	1.0007	-	-	-

Table 3. Electric parameters (open circuit voltage, V_{oc} , short circuit current density, J_{sc} , maximum power, P_{max} , fill factor, FF , photovoltaic conversion efficiency, η) of typical DSSC measured under standard illumination conditions (see also Fig. 10)

Sample	V_{oc} (mV)	J (mA/cm ²)	P_{max} (μ W)	FF	η (%)
without buffer layer	590	3.17	968.4	0.660	1.23
T2X	605	8.11	1850.4	0.480	2.36
T4X	602	8.08	1966.3	0.514	2.50
T6X	597	7.81	1836.5	0.502	2.34
T8X	611	8.28	2095.0	0.528	2.67
T10X	607	7.84	1962.6	0.525	2.50

3.2. Electro-Optical measurements

The typical solar cell parameters resulting from the electro-optical measurements performed on DSSC fabricated on FTO as well as with various numbers of spin-coated buffer layers on FTO, are displayed in Table 3 whereas the I-V curves are illustrated in Fig. 10.

The first observation is that the photovoltaic conversion efficiencies, η , obtained for DSSCs made with spin coated photo electrodes are between 2.38 % (for cells with 6 layers) and 2.67 % (for cells with 8 layers), which is almost twice the efficiency obtained for a cell without an intermediate layer. We note that the open-circuit voltage does not vary significantly. Therefore, crucial in determining the higher efficiency is the much larger short-circuit current density. The introduction of the buffer layer leads to an increasing of J_{sc} , from 3.17 mA/cm² for cells without buffer layer, to 8.28 mA/cm² for T8X.

A second observation is that the filling factor is the highest for the device without a buffer layer. The I-V curves reveal a relatively high equivalent series resistance given by the slope of the curve when the current density approaches zero. The shunt resistance given by the slope close to the short-circuit current, which is almost horizontal, is high, as desired.

Finally, even though the differences between the various layer thicknesses are small, the better characteristics obtained for the T8X sample, with an efficiency of 2.67% suggest that there is an optimum buffer layer thickness.

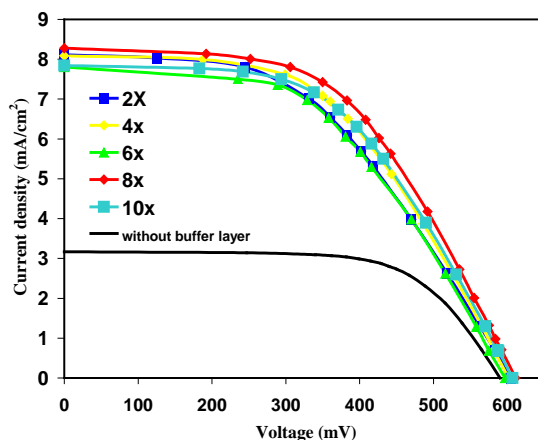


Fig. 10 Current-voltage curves for typical dye-sensitized solar cells fabricated with T2X (square), T4X (diamond), T6X (triangle), T8X (gray circle), T10X (empty circle) and without buffer layer (line) photoelectrodes

To better understand these results it is useful to start from the basic desirable and detrimental processes that take place in the DSSCs. As previously shown by other authors[26], the desirable processes are *i)* charge injection into TiO₂, *ii)* charge diffusion to FTO and *iii)* dye regeneration, whereas the detrimental processes are: *iv)* luminescence or nonradiative decay, *v)* back transfer to dye, and *vi)* charge interception by electrolyte). From this perspective, the introduction of a buffer layer increases the series resistance, R_s , due to both interface effects and the larger buffer layer thickness. This is reflected in the deviations from verticality in the shape of the I-V curve near the open-circuit point and in the lower values of the FF.

The higher J_{sc} for the devices with the buffer layer is likely due to increased charge transfer and lower contact resistance at the interface with the FTO glass when the buffer layer is present. On the other hand, the lower FF suggests that the thicker buffer film increases the series resistance.

4. Conclusions

Our study started from the assumption that spin-coated TiO₂ buffer layers would improve the performance of DSSCs. For that purpose, we fabricated DSSCs with photoelectrodes with up to 10 spin-coated layers.

The film thickness measurements showed that the total film width correlates well with the number of spin-coated layers, although the error bars are quite large due to nonuniformity of the film. The fitting to a straight line indicated that the average width of one layer is ~33 nm.

The associated SAED patterns and HRTEM images revealed the anatase structure of titania nanoparticles. The crystallite size, determined from TEM investigations, lead to average values ranging between 13 nm to 27 nm.

Electro-optical measurements carried out under standard AM 1.5G conditions showed that the introduction of a buffer layer at the interface increases significantly the short circuit current density and doubles the efficiency of the photovoltaic conversion with respect to the cells without the buffer layer. We proposed as an explanation of the better performance that the buffer layer improves the charge transfer and lowers the contact resistance at the FTO/TiO₂ interface possibly by preventing the direct contact between the electrolyte and the FTO.

Encouraged by the present study we plan to expand our exploration of the role of the buffer layer on DSSC performance by using pulsed laser deposition instead of spin coating [27]. If a simple method such as spin-coating can improve significantly the operation of the solar cell, the more uniform films obtained by means of laser deposition should lead to further improvements.

Acknowledgments

The authors acknowledge the financial support from CNCS/UEFISCDI under the contract PN2-ID-PCE-304/2011.

References

- [1] R. R. Søndergaard, M. Hösel, F. C. Krebs, Journal of Polymer Science Part B: Polymer Physics **51**, 1 (2013).
- [2] A. G. Emslie, F. T. Booner, L. G. Peck, J. Appl. Phys. **29**, 5 (1958)

- [3] D. Meyerhofer, *J. Appl. Phys.* **49**, (7) 1978.
- [4] K. Norrman, A. Ghanbari-Siahkali, N.B. Larsen, **101**, (2005).
- [5] D.W. Schubert, T. Dunkel, *Mat. Res. Innovat.* **7**, (2003).
- [6] H. Yu, S.Q. Zhang, H.J. Zhao, G. Will, P.B. Liu, *Electrochim. Acta* **54**, 5 (2009).
- [7] A.O.T. Patrocínio, L.G. Paterno, N.Y.M. Iha, *J. Photochem. Photobiol. A* **205**, 1 (2009).
- [8] S. Ito, T.N. Murakami, P. Comte, P. Liska, C. Grätzel, M.K. Nazeeruddin, M. Grätzel, *Thin Solid Films* **516**, 4 (2008).
- [9] P.Wang. , S.M. Zakeeruddin, P. Comte, R. Charvet, R. Humphry-Baker, M. Grätzel, *J. Phys. Chem. B* **107**, 51 (2003).
- [10] J.H. Kim, K.J. Lee, J.H. Roh, S.W. Song, J.H. Park, I.H. Yer, B.M. Moon, *Nanoscale Research Letters* **7**, **1** (2012) 11.
- [11] B. Yoo, K. J. Kim, S.Y. Bang, M.J. Ko, K. Kim, N.G. Park, *Journal of Electroanalytical Chemistry* **638**, 1 (2010).
- [12] Akihiko Hattori, Koji Shimoda, Hiroaki Tada, and Seishiro Ito, *Langmuir* **15**, 16 (1999).
- [13] M. Lira-Cantu, F.C. Krebs, *Solar Energy Materials & Solar Cells* **90**, 14 (2006).
- [14] T.Q. Liu, O. Sakurai, N. Mizutani, M. Kato, *J. Mater. Sci.* **21**, 10 (1986).
- [15] M.H. Aslana, A.Y. Oral, E. Men-sur, A. Gül, E. Başarana, *Solar Energy Materials & Solar Cells* **82**, 4 (2004).
- [16] M. Hocevar , U. Opara Krasovec , M. Berginc, G Drazic, N. Hauptman, M. Topic, *J Sol-Gel Sci Technol* **48**, (2008).
- [17] U. Opara Krasovec, M. Berginc, M. Hocevar, M. Topic, *Sol. Energy Mater. Sol. Cells* **93**, (2009).
- [18] M. K. Nezeeruddin, A. Kay, I. Rodicio, R. Humphry-Baker, E. Muller, P. Liska, N. Vlachopoulos, and M. Gra'tzel, *J. Am. Chem. Soc.* **115**, 14 (1993).
- [19] K.R. Millington, K.W. Fincher, A.L. King, *Sol. Energy Mater. Sol. Cells* **91**, 17 (2007).
- [20] G. P. Smestad, M Gratzel, *J. Chem. Educ.* **75**, 6 (1998).
- [21] A. Georgescu, G. Damache, and M. A. Gîrțu, *J. Optoelectron. Adv. Mater.* **10**, 11 (2008).
- [22] P. Uthirakumar, C.-H. Hong, *Material Characterization* **60**, 11 (2009).
- [23] M. Grätzel, *Nature* **414**, 6861 (2001).
- [24] N. Matin, C. Rousselot, D. Rondot, *Thin Solid Films* **300**, 1 (1997).
- [25] R. Alexandrescu, I. Morjan, M. Scarisoreanu, R. Birjega, E. Popovici, I. Soare, L. Gavrilă-Florescu, I. Voicu, I. Sandu, F. Dumitrache, G. Prodan, E. Vasile, E. Figgemeier, *Thin Solid Films* **515**, 24 (2007).
- [26] T.W. Hamann, R.A. Jensen, A.B.F. Martinson, H. Van Ryswykac, J.T. Hupp, *Energy Environ. Sci.* **1**, 1 (2008).
- [27] J. Lungu, G. Socol, C. I. Oprea, G. E. Stan, N. Ștefan, C. Luculescu, A. Georgescu1, G. Popescu-Pelin, G. Prodan, V. Ciupină,4, M A. Gîrțu, I. N. Mihăilescu, Growth of TiO2 buffer layers for dye sensitized solar cells, to be published.